A Robust Non Linear Control Scheme for Single Phase Active Multi Level Rectifier Subject to Voltage Input Sags

Harisha B
M. Tech (EPS),
Department of EEE,
St. Martin's Engineering College,
Hyderabad, Andhra Pradesh

K. Rama
Assistant Professor,
Department of EEE,
St. Martin's Engineering College,
Hyderabad, Andhra Pradesh

Abstract

In this paper, a robust nonlinear controller is proposed for the single-phase active multilevel rectifier (SPAMR) subject to voltage input sags. The controlling scheme is based on the input– output model of the rectifier system combined with exact linearization achieved via Fuzzy and generalized proportional-integral (GPI) control. The fuzzy plus GPI controller provides enhanced robustness for the SPAMR against unexpected voltage sags and load changes. The main contribution of this paper resides on avoiding the need for voltage sags detection algorithms while improving the dynamic response of the SPAMR. Simulation results obtained on a 1-kVA SPAMR using MATLAB/ Simulink and THD also analyzed.

Index Terms—*Active multilevel rectifier, generalized proportional-integral (GPI) controllers, robust nonlinear control,*
sag compensation

1. Introduction

In recent years, the harmonic pollution in power systems due to loads not Linear has become a serious problem. As a result of the current injection distorted grid, power quality has been diminished, the above is seen reflected in problems such as voltage distorted in the common connection point under power factor on sensitive loads malfunction[2], failure critical loads, among others, making the use of energy-inefficient. These problems have led to the generation pattern of standards and specifications such CFE recommendation as L0000-45 based on the IEEE 519, for the case of Mexico, created with the objective of reducing overall levels of distortion. Typical examples of non-linear loads are energy conversion systems, where the controlled rectifiers filtering capacitors, one of the most common causes of harmonic distortion found in both the industrial and domestic applications.

At present a variety of processes require power generation Direct current (DC) from a source of alternating current (ac), this transformation is usually achieved through a rectifying circuit, which is constituted by a diode bridge does not controlled and a capacitor as filter element as shown in Fig 1. Although the advantages of this system, among which are simplicity and low cost, important to mention the problems it creates, such as voltage sag, increased harmonic distortion current and low power factor.

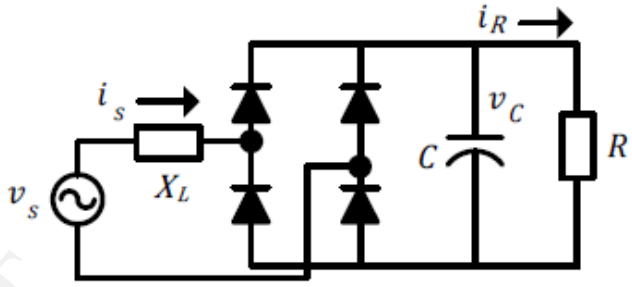

Fig.1. Basic Circuit rectification

2. Single Phase Active Multilevel Rectifier

The problems associated with rectification systems exposed to this point, is Own uncontrolled rectifier circuit. Furthermore, the active rectifier circuits possess the ability to reduce these problems. Specifically, the Single Phase active multilevel converter (SPAMR) shown in Figure2 is capable of correcting factor regulate power and dc voltage given by the sum of the voltages across each capacitor, i.e, $V_{dc}= V_{c1}+ V_{c2}$

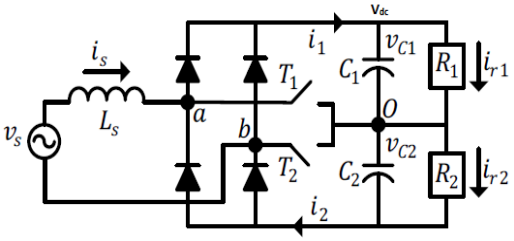

Figure 2. Single Phase Active Multilevel Rectifier (SPAMR)

This topology consists of a non-controlled diode bridge, an inductor elevator two capacitors and two bidirectional switches. Appropriately switching the switches, it is possible to regulate the dc voltage at the desired operating point, keeping the free input current harmonics and high power factor. These features make this system an element that efficiently leverages the power provided by the mains without deteriorating the

quality thereof as proven in research work in general are discussed in the next section.

In the literature there have been several control schemes for the SPAMR, between which the main feature is the power factor correction, decreasing harmonic distortion in the input current and dc voltage regulation.

2.1.Analysis Of Single Phase Active Multilevel Rectifier

2.2 Modes of Operation

SPAMR behavior can be divided into four modes, which depend on the state of the switches and. Figure 2.2 shows the equivalent circuits. Each mode of operation offers different characteristics, so that the switching of the switches can increase or decrease the input current and load or unload voltages in the capacitors. Such features can reduce the level of distortion input current and dc voltage to maintain a desired operating point.

2.2.1 Mode 1[T1 Open, T2 Open]

Because the lifting frames of the circuit, the absolute value decreases and the voltage at both capacitors increase its value. The circuit corresponding to this mode of operation shown in Figure 2.2 (a) and the equation describing its behavior is

$$v_s = L_s \frac{di_s}{dt} + v_{C1} + v_{C2}\,, \qquad i_s > 0$$
$$v_s = L_s \frac{di_s}{dt} - (v_{C1} + v_{C2})\,, \qquad i_s < 0 \tag{2.1}$$

2.2.2 Mode 2[T1 Open, T2 Closed]

In the second mode of operation the capacitor is charged and the voltage increases value when the input current is positive. Moreover, the capacitor and charged voltage increases in value when the input current is negative. The equation describes their behavior

$$v_s = L_s \frac{di_s}{dt} + v_{C1}\,, \qquad i_s > 0$$
$$v_s = L_s \frac{di_s}{dt} - v_{C2}\,, \qquad i_s < 0 \tag{2.2}$$

2.2.3 Mode 3 [T1 Closed, T2 Open]

In the third mode of operation the capacitors and loaded when the current input is positive and negative, respectively. Similarly voltages and increase in value according to the sign of the input current. The and the equation describing its behavior is:

$$v_s = L_s \frac{di_s}{dt} + v_{C2}\,, \qquad i_s > 0$$
$$v_s = L_s \frac{di_s}{dt} - v_{C1}\,, \qquad i_s < 0 \tag{2.3}$$

2.2.4 Mode 4 [T1 Closed, T2 Closed]

The latter mode of operation is the absolute value of the input current increases because the voltage between terminals ab circuit equals zero. The equation that describes the behavior is

$$v_s = L_s \frac{di_s}{dt} \tag{2.4}$$

Based on the above analysis, is presented in Table 2.1, it shows the level of voltage between terminals ab of the SPAMR for each mode depending on the sign of the input current

I_s	T_1	T_2	V_{ab}
Positive values	0	0	$V_{c1}+V_{c2}$
	0	1	V_{c1}
	1	0	V_{c2}
	1	1	0
Negative values	0	0	$-(V_{c1}+V_{c2})$
	0	1	$-V_{c2}$
	1	0	$-V_{c1}$
	1	1	0

Table 2.1.Voltage between terminals ab of the SPAMR

2.3 Mathematical Model

The differential equations describing the dynamics of the SPAMR are given by

$$L_s \frac{d}{dt} i_s = v_s - v_{ab}$$
$$C_1 \frac{d}{dt} v_{C1} = i_1 - i_{r1}$$
$$C_2 \frac{d}{dt} v_{C2} = i_2 - i_{r2} \quad (2.5)$$

Then

$$v_{ab} = \frac{sgn(i_s)+1}{2}[v_{C1}(1-T_1)+v_{C2}(1-T_2)] + \frac{sgn(i_s)-1}{2}[v_{C1}(1-T_2)+v_{C2}(1-T_1)]$$

$$i_1 = \frac{sgn(i_s)+1}{2}(1-T_1)i_s + \frac{sgn(i_s)-1}{2}(1-T_2)i_s$$

$$i_2 = \frac{sgn(i_s)+1}{2}(1-T_2)i_s + \frac{sgn(i_s)-1}{2}(1-T_1)i_s \quad (2.6)$$

2.3.1 Simplification at Three Levels

In order to obtain a model to derive the control algorithm proposed in this thesis, it is assumed that the switches simultaneously switched i.e. $T_1=T_2=T$. Thus use two of the four operating modes SPAMR thus, the voltage generated between terminals ab is three levels as shown in Table2.2.

I_S	T_1	T_2	V_{AB}
POSITIVE	0	0	$V_{C1}+V_{C2}$
	1	1	0
NEGATIVE	0	0	$-(V_{C1}+V_{C2})$
	1	1	0

Table 2.2. Voltage between terminals ab of the SPAMR when $T_1=T_2=T$

Moreover, it is considered that the load resistors are equal, i.e.$R_1=R_2=R$, Likewise, the capacitors $C_1=C_2=C$. In this way we obtain the state as the sum of V_{c1} and V_{c2} adding the effect of the resistance and inductor associated with the SPAMR model can be rewritten as

$$L_s \frac{d}{dt} i_s = v_s - v_{ab} - R_s i_s \quad (2.7)$$

$C\frac{d}{dt}V_{dc} = 2i - i_R$

Then

$V_{ab} = sgn(i_s)(1-T)V_{dc}$

$$i = i_1 = i_2 = sgn(i_s)(1-T)i_s \quad (2.8)$$

$i_R = \frac{Vdc}{R}$

Finally, we define the switching function And obtain the dynamic model of SPAMR represented by: r = sgn (i_S) (1-T): $\mathbb{R} \rightarrow$ {-1, 0, +1} where is obtained using the technique of pulse width modulation sinusoidal (SPWM).

$$\begin{bmatrix} Ls\frac{d}{dt}is \\ C\frac{d}{dt}Vdc \end{bmatrix} = \begin{bmatrix} -Rs & -\tau \\ 2\tau & -1/R \end{bmatrix} \begin{bmatrix} is \\ Vdc \end{bmatrix} + \begin{bmatrix} 1 \\ 0 \end{bmatrix} V_s \quad (2.9)$$

2.4 Average Model

The state equations in (2.9) do not represent a useful model of the SPAMR because the switching function is provided within the set of discrete {-1,0,+1} Causing the is bilinear model (solid parts). Therefore, the dynamical model obtained in previous section is considered as a average (The average pattern obtained by averaging the dynamic model by switching period under assumption that the switching frequency is infinite) model assuming switching to a high frequency and redefining it as a continuous function u: R $\rightarrow$ {-1, +1} sufficiently differentiable.

Thus, the average model SPAMR is:

$$\begin{bmatrix} Ls\frac{d}{dt}is \\ C\frac{d}{dt}Vdc \end{bmatrix} = \begin{bmatrix} -Rs & -u \\ 2u & -1/R \end{bmatrix} \begin{bmatrix} is \\ Vdc \end{bmatrix} + \begin{bmatrix} 1 \\ 0 \end{bmatrix} V_s \quad (2.10)$$

On the other hand, the GPI has been widely applied to obtain dc dc converters satisfactory results. Based on this background, 2.10) is mapped to a framework of synchronous reference through dq transformation phase. Thus the average pattern SPAMR contains only dc signals so that it can be seen as a dc-dc converter elevator.

2.5 Dq Model

According to the theoretical principle of single phase dq transformation , is generated orthogonal imaginary circuit, this imaginary circuit is composed of the same components the actual circuit with the difference that all steady-state variables are delayed 90

° from their counterparts in the real circuit. Thus, you get a frame of reference stationary and applying the transformation matrix:

$$\boldsymbol{T} = \begin{bmatrix} sin(\omega t) & -cos(\omega t) \\ cos(\omega t) & sin(\omega t) \end{bmatrix} \quad (2.11)$$

Variables are obtained in the dq synchronous reference frame where grid frequency is in rad /s.
The SPAMR, the real and imaginary signals are

$$\boldsymbol{I_s} = \begin{bmatrix} i_s^{re} \\ i_s^{im} \end{bmatrix}, \qquad \boldsymbol{V_s} = \begin{bmatrix} v_s^{re} \\ v_s^{im} \end{bmatrix}, \qquad \boldsymbol{U} = \begin{bmatrix} u^{re} \\ u^{im} \end{bmatrix} \quad (2.12)$$

Using the above vectors in the model (2.10), the equation of the input current can be rewritten in vector form as:

$$L_s \frac{d}{dt} I_s = - R_s I_s - V_{dc} U + V_s \quad (2.13)$$

Applying the transformation matrix T has:

$$T\left[Ls \frac{d}{dt} is\right] \quad = T[- RsIs - V_{dc}U + Vs] \quad (2.14)$$
$$V_{dc}$$

Transforming the left side of the above equation, taking the derivative of matrix product TI_s:

$$L_s \frac{d}{dt}(\boldsymbol{TI_s}) = \boldsymbol{T}\left[L_s \frac{d}{dt}\boldsymbol{I_s}\right] + \left[L_s \frac{d}{dt}\boldsymbol{T}\right]\boldsymbol{I_s} \quad (2.15)$$

then:

$$\boldsymbol{T}\left[L_s \frac{d}{dt}\boldsymbol{I_s}\right] = L_s \frac{d}{dt}(\boldsymbol{TI_s}) - \left[L_s \frac{d}{dt}\boldsymbol{T}\right]\boldsymbol{I_s} \quad (2.16)$$

Substituting (2.16) in (2.14) yields the equation of the input current under dq synchronous reference:

$$L_s \frac{d}{dt}(\boldsymbol{TI_s}) = \left[L_s \frac{d}{dt}\boldsymbol{T}\right]\boldsymbol{T^{-1}TI_s} - R_s TI_s - v_{cd}TU + TV_s \quad (2.17)$$

$$L_s \frac{d}{dt} I_s^{dq} = L_s \Omega I_S^{dq} + V_s^{dq} - R_s I_S^{dq} - U^{dq} V_{dc}$$

Where

$$\Omega = \left[\frac{d}{dt}T\right]T^{-1} = \begin{bmatrix} 0 & \omega \\ -\omega & 0 \end{bmatrix} \quad (2.18)$$

$$I_s^{dq} = \begin{bmatrix} i_s^d \\ i_s^q \end{bmatrix}, \qquad V_s^{dq} = \begin{bmatrix} v_s^d \\ v_s^q \end{bmatrix}, \qquad U^{dq} = \begin{bmatrix} u^d \\ u^q \end{bmatrix}$$

Now, using the vectors and in (2.10), the dc voltage equation can be rewritten in vector form as:

$$C \frac{d}{dt} Vdc = U^T I_s - \frac{1}{R} V_{dc} \quad s(2.19)$$

Observation: The above equation implies that adding imaginary product to Voltage equation in the model (2.10), the dc component doubles its value while the voltage ripple disappears due to cancellation between the components of actual signals ac and imaginary.

Applying a transformation matrix T (2.19) yields:

$$C \frac{d}{dt} Vdc = (T^{-1} T U)^T T^{-1} T I_s - \frac{1}{R} V_{dc} \quad (2.20)$$

$$C \frac{d}{dt} Vdc = (T^{-1} U^{dq})^T T^{-1} I_s^{dq} - \frac{1}{R} V_{dc} \quad (2.21)$$

using matrix properties:

$$(\boldsymbol{T^{-1}U^{dq}})^T = (\boldsymbol{U^{dq}})^T(\boldsymbol{T^{-1}})^T \quad (2.22)$$

$$\mathbf{T^{-1}=T^T}$$

Equation (2.21) takes the form

$$C \frac{d}{dt} Vdc = (U^{dq})^T T T^{-1} I_s^{dq} - \frac{1}{R} V_{dc} \quad (2.23)$$

Where TT^{-1} represents an identity matrix; thus, the equation for the dc voltage is rewritten as

$$C \frac{d}{dt} Vdc = (U^{dq})^T I_s^{dq} - \frac{1}{R} V_{dc} \quad (2.24)$$

Finally the complete model of the SPAMR in the dq synchronous reference frame is

$$L_s \frac{d}{dt} i_s^d = \omega L_s i_s^q - R_s i_s^d + v_s^d - v_{dc} u^d$$
$$L_s \frac{d}{dt} i_s^q = -\omega L_s i_s^d - R_s i_s^q + v_s^q - v_{dc} u^{dq} \quad (2.25)$$
$$C \frac{d}{dt} v_{dc} = -\frac{1}{R} v_{dc} + i_s^d u^d + i_s^q u^q$$

3. Control Objectives

The control objectives are
- Stabilize the dc voltage at the desired operating point.
- Reduce the THD of the input current.
- Correct the power factor.

which must be met even in the presence of disturbances in the input source, and considering an unknown current demand.
As concluded in the previous chapter, the control objectives are met using the schemes proposed, but the performance thereof is to shocks poor, therefore, is the task of GPI provide robustness to the system, for it is used system model in the presence of disturbances.

3.1. Nonlinear Control & GPI

Similarly to the previous section, the controller is implemented using nonlinear GPI is obtained for the current loop and using again the same outer loop voltage.

3.3.1. Current Loop

Using the control law in the perturbed model, the closed loop dynamics output vector is reduced to an integrator

$$\dot{y} = v + \mathcal{O}_1(t^{p-1}) \tag{3.1}$$

Where $V = \begin{bmatrix} v_{12} \\ v_{22} \end{bmatrix}$ And $\omega_1(t^{p-1}) = \begin{bmatrix} v_p^d \\ v_p^q \end{bmatrix}$.

Defining the error control signals and outputs as

$$e_v = v - v^*$$

$$e_y = y - y^* \tag{3.2}$$

Where $V^* = \dot{Y}^*$ the error dynamics is given by

$$\dot{e}_y = e_v + \mathcal{O}_1(t^{p-1}) \tag{3.3}$$

Assuming $\omega_1(t^{p-1})$ disturbance is well approximated by a polynomial of second order (p-1=2), GPI controller third order

$$e_v = -k_{c23}e_y - k_{c22}\int e_y - k_{c21}\iint e_y - k_{c20}\iiint e_y \tag{3.4}$$

the system provides robustness with respect to perturbations in the input voltage.
The block diagram o is shown in Fig. 3.1.

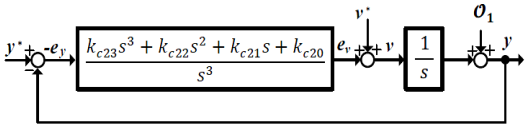

Figure 3.1 GPI current controllers for SPARM

From the diagram in Figure 3.1, the transfer functions for each output taking ω_1 as a disturbance are

$$\frac{x_1(s)}{x_1^*(s)} = \frac{k_{c23}s^3 + k_{c22}s^2 + k_{c21}s + k_{c20}}{s^4 + k_{c23}s^3 + k_{c22}s^2 + k_{c21}s + k_{c20}} \tag{3.5}$$

$$\frac{x_2(s)}{x_2^*(s)} = \frac{k_{c23}s^3 + k_{c22}s^2 + k_{c21}s + k_{c20}}{s^4 + k_{c23}s^3 + k_{c22}s^2 + k_{c21}s + k_{c20}}$$

Nominal control input $v^*=0$ because $y^*$is constant and the characteristic polynomial

$$p_{12,22}(s) = s^4 + k_{c23}s^3 + k_{c22}s^2 + k_{c21}s + k_{c20} \tag{3.6}$$

Has a fully assignable pole arbitrarily. Then, selecting the coefficients

$$\{k_{c23}, k_{c22}, k_{c21}, k_{c20}\} \tag{3.7}$$

as follows, k_{c23}= 3000 k_{c22}=1000 k_{c21}=60 and k_{c20}= 1 It releases the loopCurrent about switching frequency, obtaining a decade bandwidth a lower cutoff frequency f_c=472Hz. Fig. 3.2 shows the non-linear control scheme using the controller GPI auxiliary inputs.

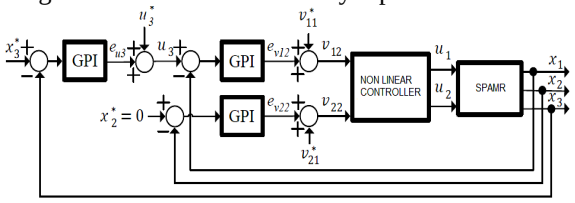

Fig.3.2. Block diagram of nonlinear control scheme & GPI for the SPAMR

3.2 Fuzzy Plus GPI in Voltage Loop

Fuzzy logic and generalized proportional-integral (GPI) controllers are use in SPAMR for sag mitigation. A simulation study of the SPAMR with GPI is studied. The Fuzzy rules and the inference mechanism of the fuzzy logic controller (FLC) are evaluated by using conventional rule-lookup tables that encode the control knowledge in a rules form. The

performance assessment of the studied position controllers is based on dynamic response and error integral criteria. The results obtained from the FLC are not only superior in the output voltage, but also much better in reducing the total harmonic distortion

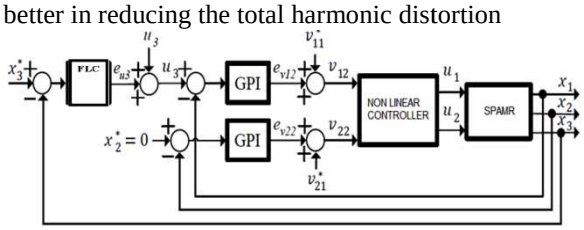

Fig.3.3Block diagram of nonlinear control scheme Fuzzy & GPI for the SPAMR

3.2.1 Rule Viewer

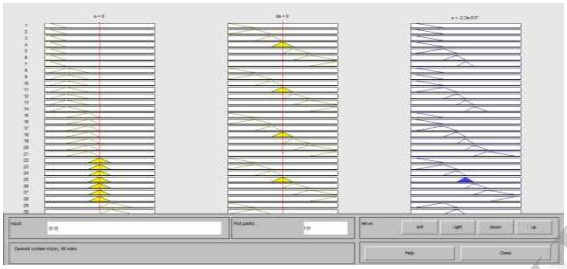

3.2.2 Surface Viewer

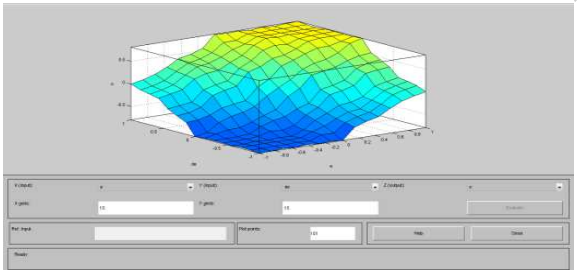

4.Simulation Results

Two types of tests were proposed to validate the nonlinear control scheme ability to achieve the control objectives. The first one is concerned with the quality of the steady-state behavior and the second one is the ability to compensate voltage sags without using detection algorithms. The performance of the scheme on the entire operation range was also tested. For this purpose, an ac mains voltage sag was induced at the same time of several load changes.

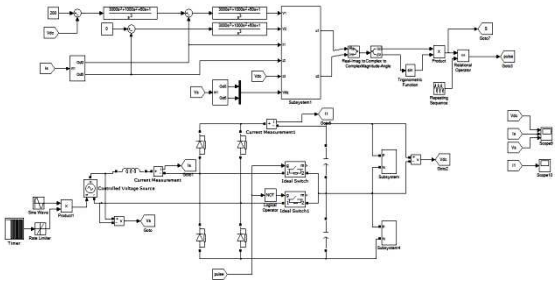

Simulink model of SPAMR
(non linear load with GPI controller)

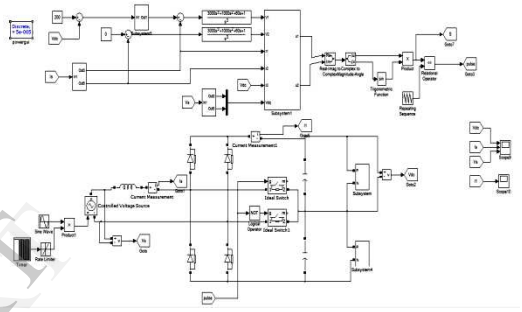

Simulink model of SPAMR
(non linear load with GPI and Fuzzy controller)

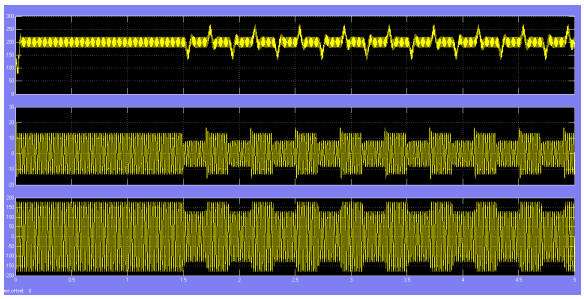

Simulation results of SPAMR with GPI

(non linear load)
(a) output voltage (b) input current (c) input voltage

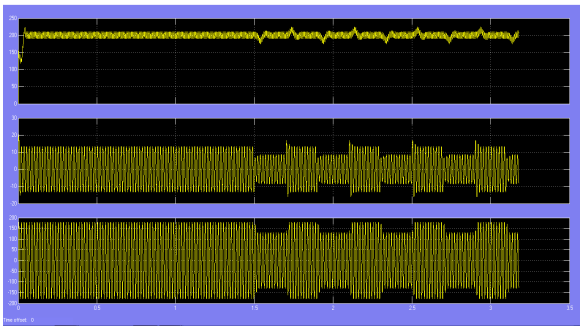

Simulation results of SPAMR Fuzzy and GPI
(non linear load)
(a) output voltage (b) input current (c) input voltage

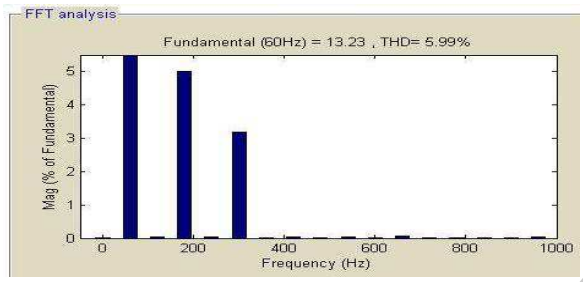

THD of Non Linear Load With GPI Controller

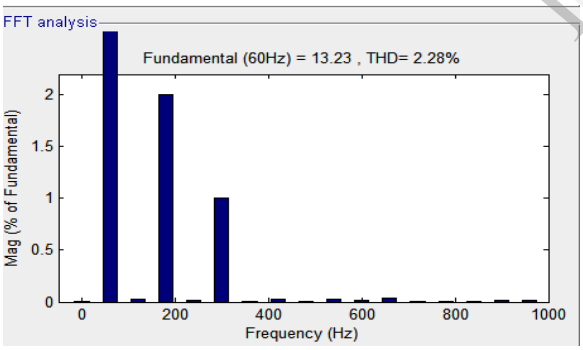

THD of Non Linear Load With Fuzzy Plus GPI Controller

5. Conclusion

A nonlinear control scheme for an SPAMR has been proposed. The main motivations for this proposal were to provide to the SPAMR with the capability to work well in the operation range while exhibiting a good dynamic behavior. At the same time, this approach enjoys added robustness properties with respect to ac mains voltage perturbations and dynamical load changes while eliminating the need for a sag detection algorithm. This is, particularly, relevant from a power electronics viewpoint. It is important to mention that the controller parameters, both, in the simulations and in the experimental tests, were kept to be the same.

6. References

1] H. G. Sarmiento and E. Estrada, “A voltage sag study in an industry with adjustable speed-drives,” IEEE Ind. Appl. Mag., vol. 2, no. 1, pp. 16–19, Jan./Feb. 1993.

[2] M. H. Bollen Understanding Power Quality Problems, Voltage Sags and Interruptions (Series Power Engineering), Piscataway, NJ: IEEE Press, 2000, ch. 1.

[3] J. Wang, S. Chen, and T. T. Lie, “Estimating economic impact of voltage sags,” in Proc. Int. Conf. Power Syst. Technol., 2004, pp. 350–355.

[4] Z. Yan, X. Yonghai, X. Xiangning, Z. Yongqiang, and G. Chunlin, “Powerquality disturbances identification based on dq conversion, wavelet transform and FFT,” in Proc. Power Energy Eng. Conf., 2010, pp. 1–4.

[5] M. Gonz´alez, V. C´ardenas, and R. Alvarez, “A fast detection algorithm for sags, swells, and interruptions based on digital RMS calculation and Kalman filtering,” in Proc. IEEE Int. Conf. Power Electron., 2006, pp. 1–3.

[6] C. Ngai Ho and H. S.-H. Chung, “Implementation and performance evaluation of a fast dynamic control scheme for capacitor-supported interline DVR,” IEEE Trans. Power Electron., vol. 25, no. 8, pp. 1975–1988, Aug. 2010.

[7] S. Subramanian and M. Kumar, “Interphase AC–AC topology for voltage sag supporter,” IEEE Trans. Power Electron., vol. 25, no. 2, pp. 514–518, Feb. 2010.